Study of the parametric excitation phenomenon of a slender riser using finite element method and a reduced order model

Guilherme Rocha Martins[1], Paulo Akira Figuti Enabe[1], Rodrigo Provasi[1], Alfredo Gay Neto[1]

[1]*Dept. of Structural and Geotechnical Engineering, Polytechnic School, University of São Paulo*
Avenida Professor de Almeida Prado tv. 2 n.83, 05508070, São Paulo, Brasil
guilherme.rocha.martins@usp.br, paulo.enabe@usp.br, provasi@usp.br, alfredo.gay@usp.br

Abstract. In the context of oil and gas (O&G) exploitation, risers are slender structures connecting the floating unit to the seabed. These structures experience static and dynamic loads with potentially high nonlinearities. It is relevant for O&G industry to understand the riser's mechanical behavior to improve the structure life and predict failures. In this sense, this work focuses on the analysis of the dynamical behavior of a vertical riser (represented as a vertical beam) under harmonic excitation in the top, standing for the oscillation of a floating unit. Depending on the structure's mechanical properties and on the load frequency, the parametric excitation phenomenon can take place, yielding large-amplitude lateral motion even for small vertical displacements. More specifically, the focus is on the Mathieu's instability regions, which occurs when the excitation frequency is an even multiple of the structure natural frequency. In this work, we establish a simplified analytical approach using a reduced order model (ROM), which considers an Euler-Bernoulli beam model undergoing small rotation. For this purpose, the equations of motion are obtained using the extended Hamilton's principle (EHP). By applying Galerkin's method using three sinusoidal shape functions and considering a time-spatial split, ROM's non-dimensional final equations can be obtained. Next, an in-house nonlinear FEM-based solver, called Giraffe (an acronym for "Generic Interface Readily Accessible For Finite Element") is presented and some comparative examples are performed using the ROM and the Giraffe, observing their differences and similarities. These case studies were performed considering the structure immersed in water and air, and the excitation frequency is varied to evaluate the first and the second Mathieu's instability region. The results presented good agreement in both models, with, in general, slightly larger displacements for the ROM models.

Keywords: Parametric excitation, finite element method, reduced order model, Mathieu's instability

1 Introduction

Parametric excitation is a phenomenon that occurs when one or more parameters of the equations of motion have an explicit dependence on time [1]. When this dependency takes place in the stiffness coefficient of the equation of motion, we have Hill's equation and if the stiffness time-dependency is harmonic, it is called Mathieu's equation.

Such a family of equations has been used to investigate some offshore engineering applications, like vertical risers (slender tubular structures that transport oil and gas from the seabed to floating units) and tethers of tension leg platforms (TLPs). In the last decades, many books (see e.g.: [2, 3]) and articles have invested efforts to evaluate the dynamic response of these slender structures not only with analytical and numerical approaches [4–6], but also with experimental analyses [7]. The Mathieu's instability phenomenon is also a research topic in the offshore bibliography [8, 9], with a practical interest in the principal instability, which is defined when the excitation frequency is double of the natural frequency.

It is known that the lateral motion of cables is well-described by Bessel functions. Vernizzi et al. [1] compared the usage of "Bessel-like" and trigonometric functions and pointed that the usage of a single "Bessel-like" function as a shape function, simplify results attainment like the post-critical amplitude map with less computational effort, despite the greatest mathematical difficulty in the model. In the literature one can found many works using a set of trigonometric functions [5, 10] and others "Bessel-like" [1, 11] as shape functions.

Present work starts with a brief description of the mathematical model (deeper discussions about it were made by Mazzilli et al. [10]), followed by the ROM's derivation with some highlights (more details can be found, with small differences, in Franzini et al. [7], Franzini and Mazzilli [12]) and case studies with the Giraffe and the ROM for the two first Mathieu's instability regions.

2 Mathematical Model

The model studied is illustrated in Figure 1. Considering a Bernoulli-Euler formulation under small rotation hypothesis, the strain ε and its variation $\delta\varepsilon$ at a generic point p are given by:

$$\varepsilon = w' - xu'' + \frac{1}{2}(u')^2 = \overline{\varepsilon} - xu'', \tag{1}$$

$$\delta\varepsilon = \delta w' - x\delta u'' + u'\delta u', \tag{2}$$

where $(\cdot)' = \frac{\partial(\cdot)}{\partial z}$, $(\cdot)'' = \frac{\partial^2(\cdot)}{\partial z^2}$ and $\overline{\varepsilon}$ is the axial strain. The term $\frac{1}{2}(u')^2$ takes into account the structure extensibility.

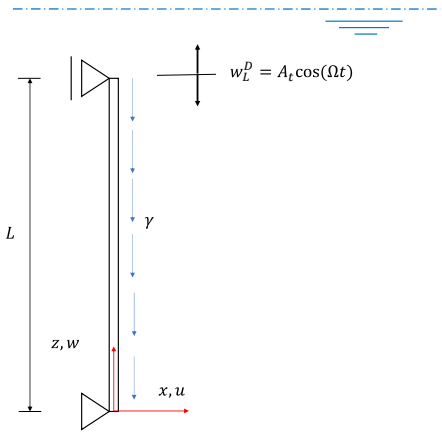

Figure 1. Representation of the vertical riser subject to an excitation at the top

Similarly to what is done by Mazzilli et al. [10] and in Franzini and Mazzilli [12], by applying the Extended Hamilton's Principle (EHP), one can obtain the coupled system of equations of motion given by:

$$\mu\ddot{u} + EIu'''' + c\dot{u} - EA\left((u'w')' + \frac{3}{2}(u')^2 u''\right) = 0\,, \tag{3}$$

$$\mu\ddot{w} + \gamma - EA\,(w'' + u'u'') = 0\,, \tag{4}$$

where EI is the bending stiffness, EA is the axial stiffness, μ is the linear mass, c is the structural damping coefficient and γ is the submerged weight. It is important to mention that the structural damping is assumed to be derived from a Rayleigh dissipation function (proportional to velocity) and acting only in the lateral direction.

Before the dynamic excitation, a static problem defines the pretension, which gives its geometric stiffness. Therefore, the motion and tension can be separated in static and dynamic terms, denoted by superscript S and D, respectively. The natural boundary condition for the static problem, defines the static top tension, T_L^S:

$$T^S(L) = T_L^S = EA\left(w' + \frac{1}{2}(u')^2\right) = EA\overline{\varepsilon}\,. \tag{5}$$

Disregarding the inertial term and integrating eq. (4), it is possible to calculate the axial strain, ϵ_0 by an average procedure [1, 10]:

$$\epsilon_0(t) = \epsilon_0 = \frac{w_L - w_0}{L} + \frac{1}{2L}\int_0^L (u')^2 dz - \frac{\gamma L}{2EA} \,. \tag{6}$$

The displacement also can be divided into a static and a dynamic component, w^S and w^D, respectively. Considering only the static problem (a vertical displacement at the top of w_L^S and no movement in the transverse direction) one can integrate the eq. (4) with respect z and, using the essential boundary condition $w(0) = 0$, obtain the static top displacement:

$$w_L^S = \frac{\gamma L^2}{2EA} + \frac{(T_L^S - \gamma L)L}{EA} \,. \tag{7}$$

Substituting eqs. (6)-(7) in eq. (3) and adding the hydrodynamic forces in the right-hand side (as done by other authors [1, 7, 11, 12]), it is possible to obtain a single equation to describe the lateral motion:

$$\mu\ddot{u} + c_1\dot{u} + EIu'''' - \gamma u' - u''T(z) - \frac{EA}{L}w_L^D u'' - \frac{EA}{2L}u''\int_0^L (u')^2 dz = -\mu_a\ddot{u} - \frac{1}{2}\rho D C_d \left|\dot{u}\right|\dot{u}. \tag{8}$$

where was used Morison's equation in the right-hand side to describe the hydrodynamic forces. Thus, there is a term in phase with the acceleration (added mass, with coefficient μ_a) and a quadratic viscous drag (with coefficient C_d). Also, ρ is the specific weight of the water and D is the structure diameter.

2.1 Reduced Order Model (ROM)

The ROM is constructed assuming a temporal-spatial separation of the response and using three modes to apply Galerkin's method. Thus, the lateral motion is given by $u = \sum_{k=1}^{3} A_k(t)\,\psi_k(z)$, where $A_k(t)$ is the generalized coordinates and $\psi_k(z)$ stands for the shape functions. In this work, in order to achieve more algebraic simplicity, it is used a set of three sinusoidal functions $\psi_k(z) = \sin\left(\frac{k\pi}{L}z\right)$, with $k = 1, 2, 3$.

Substituting the proposed solution u to eq. (8) and applying the Galerkin's method (for details see [5, 12]) it is possible to obtain a non-dimensional system of differential equations, which solution describes the ROM motion:

$$\begin{aligned}
\frac{d^2\hat{A}_1}{d\tau^2} \;+\; & \alpha_1\frac{d\hat{A}_1}{d\tau} + (\delta_1 + \epsilon_1\cos(n\tau))\hat{A}_1 + \alpha_2\hat{A}_2 + \alpha_3\hat{A}_1^3 + \alpha_4\hat{A}_2^2\hat{A}_1 + \alpha_5\hat{A}_1\hat{A}_3^2 + \\
& \Lambda_M\int_0^L \left|\frac{d\hat{A}_1}{d\tau}\psi_1 + \frac{d\hat{A}_2}{d\tau}\psi_2 + \frac{d\hat{A}_3}{d\tau}\psi_3\right|\left(\frac{d\hat{A}_1}{d\tau}\psi_1 + \frac{d\hat{A}_2}{d\tau}\psi_2 + \frac{d\hat{A}_3}{d\tau}\psi_3\right)\psi_1 dz = 0 \,, \qquad (9) \\
\frac{d^2\hat{A}_2}{d\tau^2} \;+\; & \beta_1\frac{d\hat{A}_2}{d\tau} + (\delta_2 + \epsilon_2\cos(n\tau))\hat{A}_2 + \beta_2\hat{A}_3 + \beta_3\hat{A}_1 + \beta_4\hat{A}_2\hat{A}_1^2 + \beta_5\hat{A}_2^3 + \beta_6 A_2\hat{A}_3^2 + \\
& \Lambda_M\int_0^L \left|\frac{d\hat{A}_1}{d\tau}\psi_1 + \frac{d\hat{A}_2}{d\tau}\psi_2 + \frac{d\hat{A}_3}{d\tau}\psi_3\right|\left(\frac{d\hat{A}_1}{d\tau}\psi_1 + \frac{d\hat{A}_2}{d\tau}\psi_2 + \frac{d\hat{A}_3}{d\tau}\psi_3\right)\psi_2 dz = 0 \,, \qquad (10) \\
\frac{d^2\hat{A}_3}{d\tau^2} \;+\; & \gamma_1\frac{d\hat{A}_3}{d\tau} + (\delta_3 + \epsilon_3\cos(n\tau))\hat{A}_3 + \gamma_2\hat{A}_2 + \gamma_3\hat{A}_3\hat{A}_2^2 + \gamma_4\hat{A}_3\hat{A}_1^2 + \gamma_5\hat{A}_3^3 + \\
& \Lambda_M\int_0^L \left|\frac{d\hat{A}_1}{d\tau}\psi_1 + \frac{d\hat{A}_2}{d\tau}\psi_2 + \frac{d\hat{A}_3}{d\tau}\psi_3\right|\left(\frac{d\hat{A}_1}{d\tau}\psi_1 + \frac{d\hat{A}_2}{d\tau}\psi_2 + \frac{d\hat{A}_3}{d\tau}\psi_3\right)\psi_3 dz = 0 \,, \qquad (11)
\end{aligned}$$

where ω_1 is the first-mode frequency of the immersed riser and $\mu_d = \rho\pi D^2/4$ is the water mass per unit length displaced by the riser. Also, the non-dimensional quantities are: $\tau = t\omega_1$, $n = \frac{\Omega}{\omega_1}$, $\hat{A}_k = \frac{A_k}{D}$, $C_a = \frac{\mu_a}{\mu_d}$, $\overline{\mu} = \frac{\mu_a}{\mu_d}$ and $\Lambda_M = \frac{D}{L\mu_d(\overline{\mu}+C_a)}\rho C_d$. In this way, the parameters of the ROM are showed in Table 1 and eqs. (12)-(13):

Table 1. Parameters of the ROM

$\alpha_1 = \frac{c}{\mu_d(\overline{\mu}+C_a)\omega_1}$	$\beta_1 = \alpha_1$	$\gamma_1 = \alpha_1$
$\alpha_2 = -\frac{40\gamma}{9L\mu_d(\overline{\mu}+C_a)\omega_1^2}$	$\beta_2 = -\frac{312\gamma}{25L\mu_d(\overline{\mu}+C_a)\omega_1^2}$	$\gamma_2 = \beta_2$
$\alpha_3 = \frac{d^2EA}{4\mu_d(\overline{\mu}+C_a)\omega_1^2}\left(\frac{\pi}{L}\right)^4$	$\beta_3 = \alpha_2$	$\gamma_3 = \frac{9d^2EA}{\mu_d(\overline{\mu}+C_a)\omega_1^2}\left(\frac{\pi}{L}\right)^4$
$\alpha_4 = \frac{d^2EA}{\mu_d(\overline{\mu}+C_a)\omega_1^2}\left(\frac{\pi}{L}\right)^4$	$\beta_4 = \alpha_4$	$\gamma_4 = \alpha_5$
$\alpha_4 = \frac{9d^2EA}{4\mu_d(\overline{\mu}+C_a)\omega_1^2}\left(\frac{\pi}{L}\right)^4$	$\beta_5 = \frac{d^2EA}{4\mu_d(\overline{\mu}+C_a)\omega_1^2}\left(\frac{2\pi}{L}\right)^4$	$\gamma_5 = \frac{d^2EA}{4\mu_d(\overline{\mu}+C_a)\omega_1^2}\left(\frac{3\pi}{L}\right)^4$
-	$\beta_6 = \gamma_3$	-

$$\epsilon_k = \frac{EA}{L}\left(\frac{k\pi}{L}\right)^2 \frac{A_t}{\mu_d\left(\overline{\mu}+C_a\right)\omega_1^2}\,, \tag{12}$$

$$\delta_k = \frac{EI}{\mu_d\left(\overline{\mu}+C_a\right)\omega_1^2}\left(\frac{k\pi}{L}\right)^4 + \left(\frac{k\pi}{L\omega_1}\right)^2\left(\frac{2T_L^S-\gamma L}{2\mu_d\left(\overline{\mu}+C_a\right)}\right)\,. \tag{13}$$

Despite the hydrodynamic damping, all the parameters are given by algebraic expressions, so they can be easily computed. To calculate these damping terms in eqs. (9)-(11), the model was discretized in 500 points along the span and the position of each one is evaluated at each time and each spanwise position, z^d. Thus, defining $g(z^d,\tau) = \frac{d\hat{A}_1}{d\tau}\psi_1^d + \frac{d\hat{A}_2}{d\tau}\psi_2^d + \frac{d\hat{A}_3}{d\tau}\psi_3^d$ it is possible to evaluate a new function $f_i(z^d,\tau) = \left|g(z^d,\tau)\right| g(z^d,\tau)\psi_i(z^d)$ for each hydrodynamic term in eqs. (9)-(11), using even a simple rectangular rule.

2.2 Finite Element Model – Giraffe

Giraffe implements a multibody dynamics framework, encompassing finite elements and rigid body formulations. To describe the rotations, the chosen vector parameterization is the Rodrigues rotation vector (see Gay Neto [13]). Present work uses Giraffe beam model, a Timoshenko geometrically exact formulation, with hydrostatic and hydrodynamic contributions, as described in detail by Gay Neto [6].

Giraffe input is based on text files. Thus, constructing many inputs for multiple cases can be laborious work. To help with that, a preprocessor tool, coded in C++, was used. It receives very little information about the model (such as length, specific mass, environment data), constructs the FEM model, and calls Giraffe to solve it.

3 Results

A special focus is given to the principal Mathieu's instability, when $n = \Omega/\omega_1 = 2$. The lateral motion of three highlighted points (at $1/4\,L$, $1/2\,L$, $3/4\,L$), the amplitude spectra, and the top tension time series were compared between the ROM and FEM results, considering non-immersed and immersed simulations. The present case study is based on the model already studied, with slightly different formulations, by Franzini and Neto [5], Franzini and Mazzilli [12] - which are based on a scaled model of an 8 in. commercial pipe studied by Franzini et al. [7].

The riser general properties are presented in Table 2. The gravitational field acceleration g is $9.81\ m/s^2$, the fluid specific mass ρ is $1025\ kg/m^3$, and the top vertical motion amplitude A_t is $0.02552\ m$. With these values and defining $w_L^S = 0.05\,m$, from eq. (7) one can evaluate the static top tension T_L^S. Then, it is possible to evaluate the natural undamped frequency of the first mode from eqs. (9) and (13) - like done by Franzini and Mazzilli [12].

For the Giraffe model, this setup is easily done by defining a beam of initial size L and then prescribing a known displacement at the top of w_L^S. Next, a modal analysis is performed and the natural frequencies can be evaluated. Finally, a structural damping of $1\,\%$ is defined for each model. For the ROM, it was assumed a logarithm decrement and for the FEM, a Rayleigh damping with a null mass coefficient ($\alpha = 0$). Table 3 summarizes the parameters for the ROM and FEM models, in water and air. For the ROM, the eqs. (9)-(11) were integrated using a Runge-Kutta method present in Matlab, with a time step of $\tau = 0.02$. The FEM was integrated with a Newmark scheme (which details can be read in Gay Neto [13]), using a high numerical damping ($\gamma = 0.3$ and $\beta = 0.6$) and a time step of $t = 0.02\,s$. The results are presented in Fig. 2.

First, a very good agreement between ROM and FEM results for both cases, immersed or in air, should be noted. Also, the effect of the hydrodynamic is well captured by the two models. Note that we adopted different

Table 2. General properties for the simulations

Property	Value
External diameter, D	22.2 mm
Unstretched length, L	2.552 m
Bending stiffness, EI	0.056 Nm^2
Axial stiffness, EA	1200 N
Linear mass, μ	1.19 kg

Table 3. Models specific parameters

Model	Property	Air	Water
Both	T_L $[N]$	38.41	33.44
ROM	ω_1 $[rad/s]$	5.48	4.75
	c $[Ns/m]$	0.1305	0.1130
FEM	ω_1 $[rad/s]$	5.09	4.58
	β	0.00393	0.00437

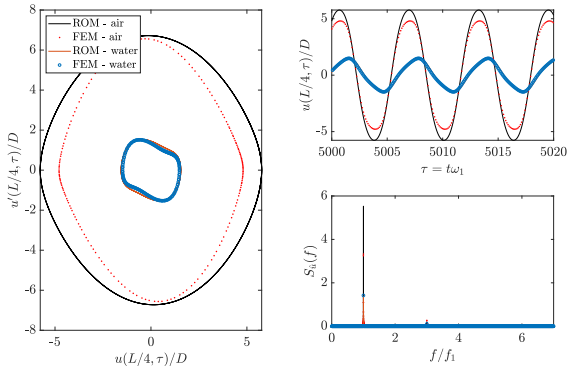

(a) Lateral displacement at $L/4$

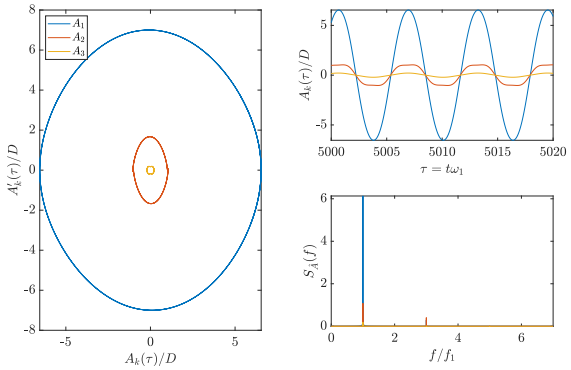

(b) Generalized coordinates from case in air

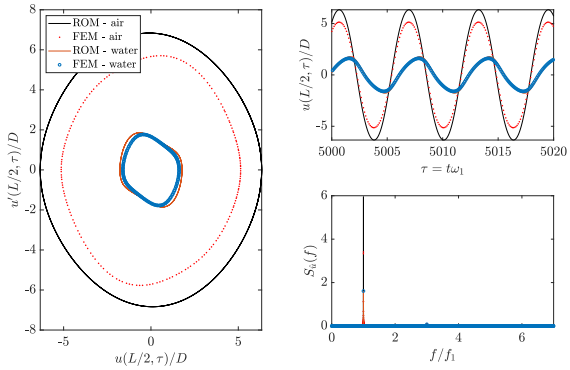

(c) Lateral displacement at $L/2$

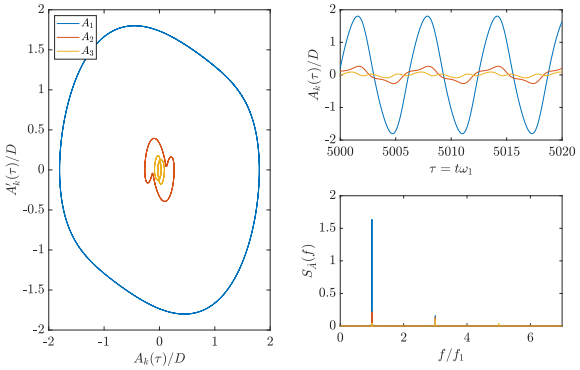

(d) Generalized coordinates from case immersed in water

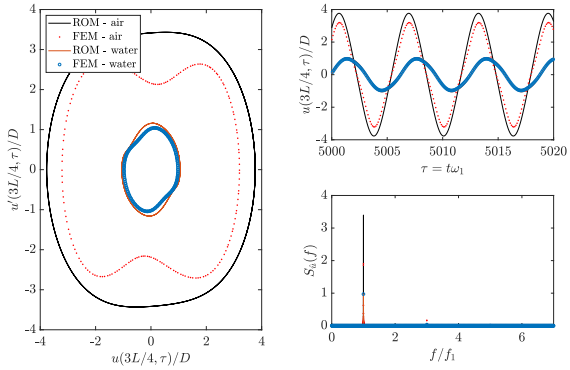

(e) Lateral displacement at $3L/4$

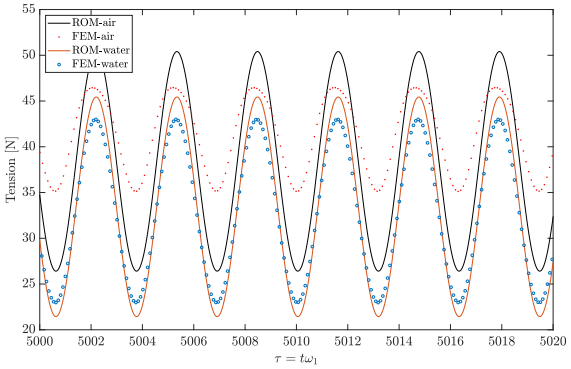

(f) Top tensions

Figure 2. Results for $n = 2$

excitation because our main goal here is to explore the Mathieu's instability. Thus, in a real case or with experimental data, when one should use the same input data in both models, the results can be slightly different because

of this difference in the natural frequencies. Vernizzi et al. [11], Franzini and Mazzilli [12] gives an idea of the expected behavior for different frequencies of excitation.

For $n = 2$, it is expected a first mode-like motion. This is reflected in the time series and spectra of the monitored points of the structure, but also in the generalized coordinates, A_i. Besides the noticeable dominance of the A_1 with the natural frequency ($f/f_1 = 1$), a curious contribution of the frequency $f/f_1 = 3$ is presented in both environmental conditions (structure in water and air) and not only for A_1.

Next, the second region of instability, $n = 4$, is simulated. For this case, we used the double of the frequencies presented in Table 3 - like mentioned by Franzini et al. [7]. Some cycles of motion are presented in Fig. 3, both ROM and FEM models, showing a good agreement between them. As expected, the structure vibrates with the shape of the second mode. Note a slightly flattening (effect of the traveling wave) in the motion due to the hydrodynamics, most recognizable in the FEM time series. Also, the locus of minimum motion along the beam span for the FEM simulation is placed a little further down than the ROM's one.

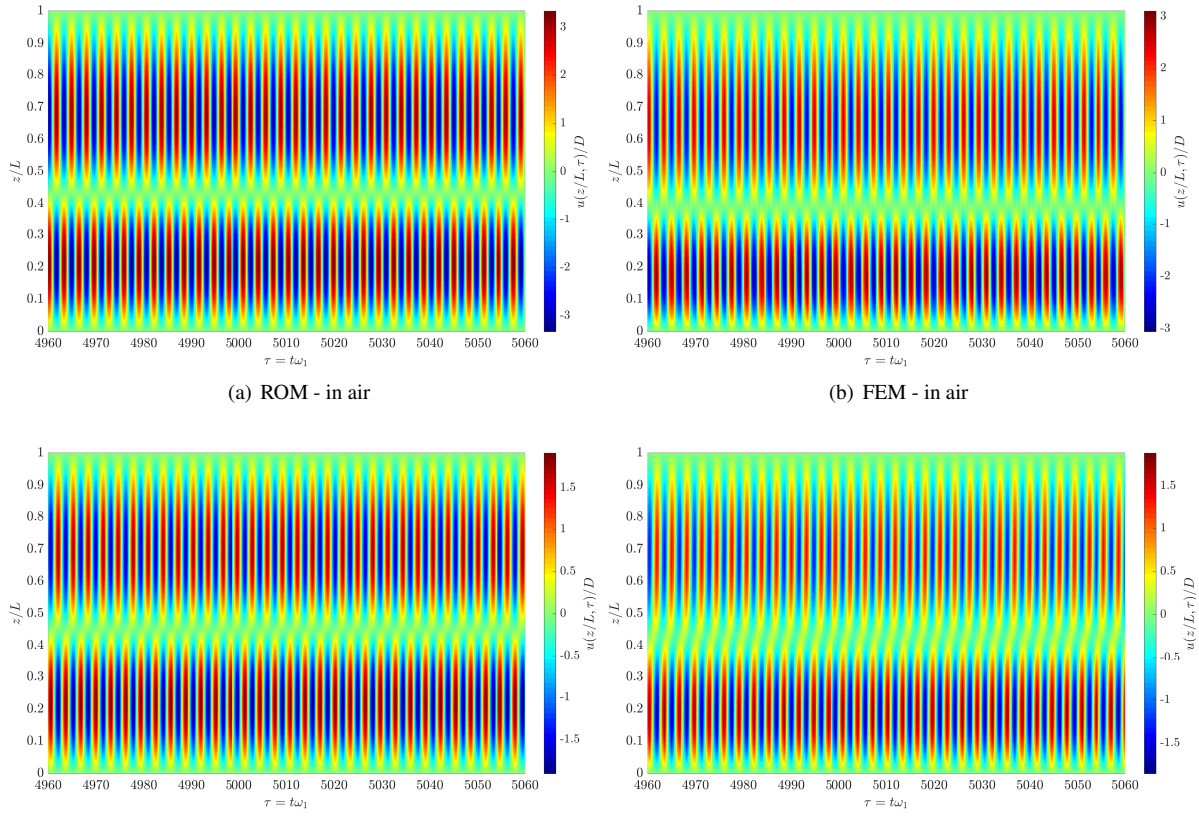

(a) ROM - in air

(b) FEM - in air

(c) ROM - in water

(d) FEM - in water

Figure 3. Scalograms for $n = 4$

4 Conclusions

This work presents some minor differences in the non-dimensional quantities of the ROM's equations from the formulations using three harmonic shape functions found in literature Franzini and Neto [5], Franzini and Mazzilli [12]. Although this had shown to have a small impact on the final results. For the case of the structure in air and $n = \Omega/\omega_1 = 2$, the present work showed a good agreement between FEM results, which shows a complementary view from what was presented by seeing Franzini and Neto [5]. For the immersed case, the hydrodynamic effect seems to minimize the, already small, difference - see Franzini and Mazzilli [12].

The hydrodynamics was well described for both models (FEM and ROM) and excitations evaluated ($n = 2$ and $n = 4$). The hydrodynamic damping reflects in the final displacement time series, but it is also noticeable in the generalized coordinates A_i, causing larger flattening in its curves than in the displacements.

Regarding to the A_i of the excitation $n = \Omega/\omega_1 = 2$ it is notable a clear dominance of A_1 in all simulations. But a contribution of the other coordinates, mainly A_2, is presented in all cases with non-negligible amplitudes, which is expected, due to the choice of harmonic shape functions over "Bessel-like" functions [1, 11]. This effect

is also seen in the results for $n = 4$, where one can note the locus of minimum motion along the riser span of the results obtained from the FEM model is located slightly below the one obtained via ROM.

Acknowledgements. The authors would like to thank Guilherme Vernizzi for some explanations about his work on parametric excitation. The first author acknowledge for the Petrobras (Petróleo Brasileiro S.A.) for the financial support during the master. The fourth author acknowledges the support of the CNPq (Conselho Nacional de Desenvolvimento Científico e Tecnológico) under the grant 304680/2018-4.

Authorship statement. The authors hereby confirm that they are the solely liable persons responsible for the authorship of this work and that all material that has been herein included as part of the present paper is either the property (and authorship) of the authors or has the permission of the owners to be included here.

References

[1] G. J. Vernizzi, G. R. Franzini, and S. Lenci. Reduced-order models for the analysis of a vertical rod under parametric excitation. *International Journal of Mechanical Sciences*, vol. 163, pp. 105–122, 2019.
[2] A. H. Nayfeh. *Nonlinear Oscillations*. John Wiley and Sons, 1979.
[3] L. Meirovitch. *Methods of Analytical Dynamics*. Dover Publications, 2003.
[4] X. Zeng, W. Xu, X. Li, and Y. Wu. Nonlinear dynamic responses of the tensioned tether under parametric excitations. The Eighteenth International Ocean and Polar Engineering Conference. ISOPE-I-08-447, 2008.
[5] G. Franzini and A. Neto. Numerical investigations on parametric excitation of a vertical beam under prescribed axial displacements. The 22nd International Congress of Sound and Vibration, 2015.
[6] A. Gay Neto. Dynamics of offshore risers using a geometrically-exact beam model with hydrodynamic loads and contact with the seabed. *Engineering Structures*, vol. 125, pp. 438–454, 2016.
[7] G. Franzini, C. Pesce, R. Salles, R. Gonçalves, A. Fujarra, and P. Mendes. Experimental analysis of a vertical and flexible cylinder in water: Response to top motion excitation and parametric resonance. *Journal of Vibration and Acoustics*, vol. 137, pp. 031010, 2015.
[8] A. N. Simos and C. P. Pesce. Mathieu stability in the dynamics of TLP's tethers considering variable tension along the length. WIT Transactions on The Built Environment, vol. 32, 1997.
[9] B. Koo, M. Kim, and R. Randall. Mathieu instability of a spar platform with mooring and risers. *Ocean Engineering*, vol. 31, n. 17, pp. 2175–2208, 2004.
[10] C. E. N. Mazzilli, C. T. Sanches, O. G. P. Baracho Neto, M. Wiercigroch, and M. Keber. Non-linear modal analysis for beams subjected to axial loads: Analytical and finite-element solutions. *International Journal of Non-Linear Mechanics*, vol. 43, pp. 551–561, 2008.
[11] G. J. Vernizzi, S. Lenci, and G. R. Franzini. A detailed study of the parametric excitation of a vertical heavy rod using the method of multiple scales. *Meccanica*, vol. 55, pp. 2423–2437, 2020.
[12] G. R. Franzini and C. E. N. Mazzilli. Non-linear reduced-order model for parametric excitation analysis of an immersed vertical slender rod. *International Journal of Mechanical Sciences*, vol. 80, pp. 29–39, 2016.
[13] A. Gay Neto. Simulation of mechanisms modeled by geometrically-exact beams using rodrigues rotation parameters. *Computational Mechanics*, vol. 59, pp. 459–481, 2017.